

I. INTRODUCTION

Spatio-temporal pattern formation in regions of the brain has been a topic of great interest for a number of years [1, 2, 4–6, 10, 12, 16, 18, 25, 29]. Because of the relative spatial scales of the patterns of activity and individual neurons, continuum models, in which space is taken as a continuous variable, are often used. The patterns studied include spatially-localised “bumps”, modelling working memory and feature

spatially approximate periodic stripes are formed by coupled groups of neurons in the prefrontal cortex [15]. Only spatially-localised patterns have previously been studied for this model [19, 21], and the oscillatory nature of the coupling function is likely to lead to novel behaviour [20].

Our goal is to use the analytical stability analysis of Hutt et al. [17] to investigate Turing instabilities in (1)–(3). Since the trigonometric functions in w have period 2π we choose a domain $x \in [-10\pi, 10\pi]$, with periodic boundary conditions. (The effects of a different domain size are discussed below). In (2) and (3), we have $b, c > 0$ and set $r = 0.095$.

The paper proceeds as follows. First, we find spatially-uniform steady states of the

ds tR1011.(s)ou

ww0.9399899i usndae find

0164.8744.8Tm [(s)w.093

that is,

$$u^* = \frac{8b(1 - e^{-10b\pi})e^{-r/(u^* - \theta)^2}}{b^2 + 1}. \quad (4)$$

Given b , (4) has one or three solutions, depending upon the value of r . Fig. 1 shows u^* as a function of r . With respect to spatially uniform perturbations, the zero and upper steady states are always stable (solid lines) and the middle steady state is unstable (dashed lines). The two nonzero steady states are destroyed in a saddle-node bifurcation as r increases.

B. Stability

To find a possible Turing bifurcation point we use the linear stability analysis of Hutt et al. [17]. Let u^* to be the upper spatially-uniform steady state found in (4) and let

$$u(x, t) = u^* + \sum_{n=-\infty}^{\infty} u_n \exp(ik_n x + \lambda_n t)$$

where $k_n = 2\pi n/L$, $L = 10$. Substituting into (1) and keeping first order terms we obtain

$$\lambda_n = -1 + W_n$$

where $f'(u^*)$ and

$$W_n = \frac{4b(b^2 + 1)[1 - (-1)^n e^{-10b\pi}]}{(b^2 + k_n^2)^2 + 2(b^2 - k_n^2) + 1}.$$

We see that $\lambda_n \in \mathbb{R}$, so no oscillatory bifurcations are expected. Bifurcations do occur when $\lambda_n = 0$, that is, when

$$W_n = 0 \Rightarrow \frac{1}{W_n} = \frac{(b^2 + k_n^2)^2 + 2(b^2 - k_n^2) + 1}{4b(b^2 + 1)[1 - (-1)^n e^{-10b\pi}]} \quad (5)$$

Since $W_n > 0$, the uniform steady state loses stability as r increases through r^* . Now $dr^*/dk_n > 0$ for $b > 1$, so in this case u^* will go unstable to a perturbation with $k = 0$, i.e. to another spatially-uniform state. When $0 < b < 1$, $r^*(k_n)$ has a minimum at $k_n = \sqrt{1 - b^2}$, and there will be a spatial pattern of wavelength k_m appearing when $k_n = k_m$, where m is the integer for which $k_m = \sqrt{1 - b^2}$.

is $k_n = 1.0$, hence $n = 10$. (Recalling that $k_n = 2n/| \Omega |$, we see that for a different domain size, periodic perturbations with n

D. The role of periodic orbits

The computational details of following periodic orbits are given in the appendix. First, we consider $b = 0.25$. The top panel of Fig. 5 shows the solution curves of 8-, 9- and 10-bump periodic solutions. Stable solutions are indicated by solid lines and unstable solutions by dashed lines. As μ is increased, 10-bump solutions are the last to be destroyed in a saddle-node bifurcation. Vertical lines indicate the value of μ for which a Turing instability occurs. The smallest value of μ for which a Turing instability can occur is for instabilities with the wavenumber $k_n = 1.0$, that is, $n = 10$. Thus a 10-bump periodic solution will always arise in a Turing instability for these parameter values. The saddle-node bifurcation of the upper and middle fixed points is given by the circles joined by solid lines. A non-trivial spatially uniform steady state cannot exist to the right of this line. To the left of the solid vertical line, a stable uniform steady state will be unaffected by a spatial perturbation. For μ between the solid vertical line and the saddle-node bifurcation vertic

$u = 0$.

The different types of behaviour are explained by Fig. 6, where we plot saddle-

Since the domain is of size 20 we take $w(x)$ to be periodic with period 20 , writing

$$w(x) = \frac{0}{2} + \sum_{p=1}^{\infty} p \cos (px/10) \quad (A2)$$

where

$$0 = \frac{2}{20} \int w(x)dx = \frac{W}{10}$$

and

$$\begin{aligned} p &= \frac{2}{20} \int \cos (px/10)w(x)dx \\ &= \frac{2b(b^2 + 1)(1 - e^{-10b\pi})}{5 \{ [b^2 + (p/10)^2]^2 + 2[b^2 - (p/10)^2] + 1 \}} \end{aligned}$$

Substituting (A1) and (A2) into (1) we have

$$\begin{aligned} \frac{a_0}{2} + \sum_{m=1}^{\infty} [a_m \cos (mnx/10) + b_m \sin (mnx/10)] = \\ \frac{0}{2} \int f[u(y)]dy + \\ \sum_{p=1}^{\infty} p \cos (px/10) \int \cos (py/10) f[u(y)]dy + \\ \sum_{p=1}^{\infty} p \sin (px/10) \int \sin (py/10) f[u(y)]dy. \end{aligned}$$

So for $p = mn$ we have

$$a_0 = \int_0^{20} f[u(x)]dx$$

$$a_m = \int_{mn}^{20} \cos (mnx/10) f[u(x)]dx$$

and

$$b_m = \int_{mn}^{20} \sin (mnx/10) f[u(x)]dx.$$

Note that since $u(x)$ is periodic with period $20/n$ we have

$$a_0 = n \int_0^{20\pi/n} f[u(x)]dx \quad (A3)$$

$$a_m = n \int_{mn}^{20\pi/n} \cos (mnx/10) f[u(x)]dx \quad (A4)$$

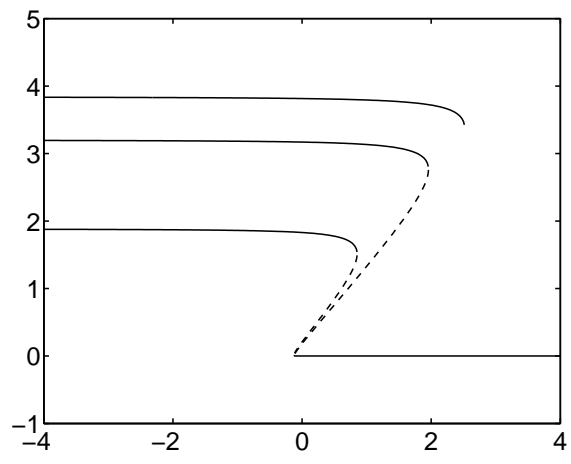
and

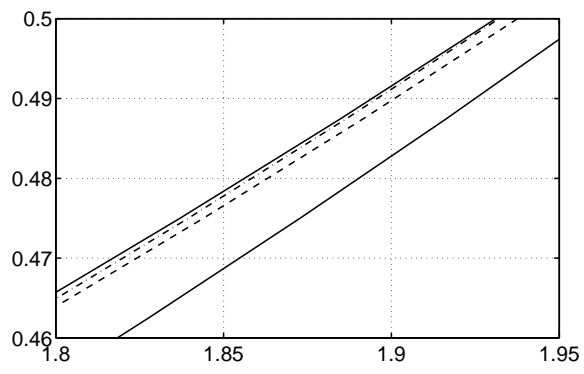
$$b_m = n \int_{mn}^{20\pi/n} \sin (mnx/10) f[u(x)]dx. \quad (A5)$$

Equations (A3)–(A5) form a set of nonlinear coupled equations. These equations do not uniquely specify the solution, since any spatial translation of $u(x)$ is also a solution. We thus pick one from this infinite family by imposing that $a_1 = 0$. We set b and ϵ , choose n , and find an initial n -bump pattern that is a solution of (1) by solving (A3)–(A5). We use the pseudoarclength continuation method [8] to find solutions as parameter values are varied. Following these patterns as ϵ is increased, we find that they are destroyed in saddle-node bifurcations, as shown in Fig. 5.

-
- [1] S. Amari, *Biol. Cybern.* **27**, 77 (1977)
 - [2] P. C. Bresslo , N. W. Bresslo and J. D. Cowan. *Neural Comput.* **12** 2473-2511 (2000).
 - [3] P. C. Bresslo , J. D. Cowan, M. Golubitsky, P. J. Thomas and M. Wiener. *Neural Comput.* **14**, 473-491 (2002)
 - [4] S. Coombes, *Biol. Cybern.* **93**, 91 (2005)
 - [5] S. Coombes and M. R. Owen, *Phys. Rev. Lett.* **94**, 148102 (2005)
 - [6] S. Coombes, N. A. Venkov, L. Shiau, I. Bojak, D. T. J. Liley, and C. R. Laing, *Phys. Rev. E* **76**, 051901 (2007)
 - [7] R. Curtu and G. B. Ermentrout, *SIAM J. App. Dyn. Sys.* **3**, 191 (2004)
 - [8] E. J. Doedel, R. C. Pa enroth, A. R. Champneys, T. F. Fairgrieve, Y. A. Kuznetsov, B. E. Oldeman, B. Sandstede and X. Wang, *AUTO 2000: Continuation and bifurcation software for ordinary differential equations (with HomCont)*, Technical Report, Caltech (2001)
 - [9] I. R. Epstein and J. A. Pojman, *An introduction to nonlinear chemical dynamics* (Oxford University Press, 1998)
 - [10] G. B. Ermentrout, *Rep. Prog. Phys.* **61**, 353 (1998)
 - [11] G. B. Ermentrout and J. D. Cowan. *Biol Cybernet* **34** 137-150, (1979).
 - [12] D. Golomb and G.B. Ermentrout. *Phys. Rev. Lett.* **86**, 4179-4182 (2001).
 - [13] J. Guckenheimer and P. Holmes, *Nonlinear oscillations, dynamical systems, and bifurcations of vector fields* (Springer-Verlag New York, Inc., 1983)
 - [14] Y. Guo and C. C. Chow, *SIAM J. App. Dyn. Sys.* **4**, 217 (2005)
 - [15] B. S. Gutkin, G. B. Ermentrout, and J. O’Sullivan, *Neurocomputing* **32–33**, 391 (2000)

- [16] D. Hansel and H. Sompolinsky. Modeling Feature Selectivity in Local Cortical Circuits. In *Methods in Neuronal Modeling: From Synapse to Networks*. Koch C and Segev I, Eds, (MIT Press, Cambridge, MA, 1998), (1998).





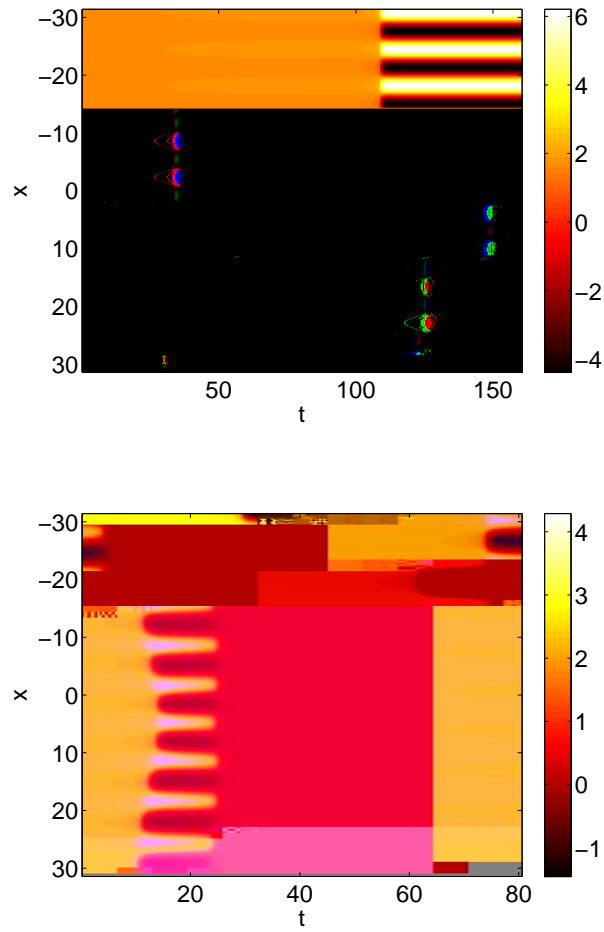


FIG. 4: (Color online) Top: A stable Turing pattern for $b = 0.25, \theta = 0.63$. Bottom: A transient Turing pattern for $b = 0.5, \theta = 1.94$. Time is plotted horizontally and space vertically. The color indicates the value of u (scale on right).

